Optimal System Design Considerations for the Ultra-Wideband Multipath Channel

Wasim Q. Malik, David J. Edwards, and Christopher J. Stevens
Department of Engineering Science, University of Oxford, Parks Road, Oxford OX1 3PJ, U.K.
Email: {wasim.malik, david.edwards, christopher.stevens}@eng.ox.ac.uk
Tel: +44 1865 283040

Abstract—**Multipath propagation in the indoor ultra-wideband channel is investigated using experimental techniques. The dependence of multipath statistics on bandwidth and centre frequency is established, and it is shown that the multipath behavior in different sub-bands is non-uniform. The multipath degrees of freedom and relative power gains are calculated. The small-scale variation in the number of multipaths over an area is characterized, and stationary wave patterns with wavelength related to signal bandwidth are reported. In the light of these findings, optimal design parameters for rake and antenna diversity systems are presented.**

Keywords- Indoor channel; multipath; rake; small-scale fading, ultra-wideband (UWB).

I. INTRODUCTION

Ultra-wideband (UWB) communications systems are defined by their large absolute or fractional bandwidths, a consequence of which is high multipath resolution capability [1, 2]. Thus a majority of the incident multipaths are resolved in a typical indoor UWB channel, depending on the propagation environment, system bandwidth and receiver sensitivity [3]. A full-band UWB system occupying a 7.5 GHz wide spectrum can resolve differential multipath delays of up to about 0.1 ns, or differential pathlengths of 4 cm. As a consequence of such high resolution, the fading and dispersion properties of the channel differ greatly from those of narrowband channels [4].

Practical system components such as antennas and filters do not provide a perfectly flat response over a very wide range of frequencies [5, 6]. Various wave propagation modes, such as scattering, diffraction and material penetration, also depend on frequency. This renders the multipath characteristics of the channel sensitive to bandwidth and frequency. Such spectrally non-uniform behavior can severely degrade the performance of both single- and multi-band UWB systems unless characterized and modeled appropriately.

The multipath effect leads to spatial small-scale fading in the time-stationary indoor channel [7]. Due to this fading, a small movement of a UWB receiver can cause the received power to vary by 5-6 dB [8]. While this is much lower than the deep fades observed in narrowband channels, it is nevertheless significant for the severely power-constrained UWB systems. This power fluctuation is directly related to the multipath arrivals at a given location and their variation with displacement. The analysis of multipath properties over a short range therefore provides an insight into the small-scale fading experienced by a receiver.

Antenna diversity can be used effectively to reduce fading and extend the coverage range of a UWB communications system [9-11]. The optimal MIMO antenna separation and the consequent improvement in link quality depends, among other factors, on the system bandwidth, operating frequency, and multipath. This raises questions about the impact of wide bandwidth on the design and performance of antenna array systems. Similarly, the SNR gain of a rake receiver depends on the number of incident and resolved multipaths, their amplitude distributions and mutual independence [12]. These are in turn determined by the multipath environment and bandwidth, which therefore have a strong impact on the performance of these specialized receivers.

This paper addresses the problem of optimal UWB communications system design for dense multipath channels. The dependence of multipath resolution on bandwidth and centre frequency is evaluated. The achievable multipath diversity gain, and the complexity of a receiver required to achieve it, is estimated using information theoretic criteria. The variation of the number of received multipaths over a planar area is investigated in order to determine the antenna spacing for a multiple-antenna receiver.

II. CHANNEL MEASUREMENT AND PROCESSING

The analysis in this paper is based on experimental results obtained from complex frequency-domain channel sounding in the UWB band (3.1–10.6 GHz). A computer-controlled vector network analyzer (VNA) system was used for this purpose in a typical office environment, as shown in Fig. 1. The distance between the transmitting antenna and the centre of the grid was 4.5 m, and the antennas were at a height of 1.5 m. Both line-of-sight (LOS) and non-line-of-sight (NLOS) scenarios were measured. A large grounded aluminum sheet was placed between the transmitter and receiver to create the blockage for NLOS. A planar grid arrangement with an automated positioner for the receiving antenna scanned a 1 m^2 area with a 0.01 m resolution. Omni-directional, vertically polarized discone antennas were used at each end of the link. A low-noise amplifier with 30 dB gain was connected to the receiving

0-7803-9152-7/05/$20.00 © 2005 IEEE

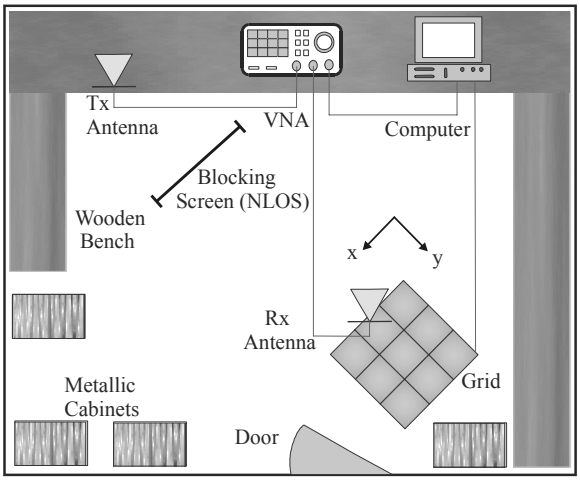

Figure 1. Indoor UWB channel measurement system with a vector network analyzer and a positioning grid

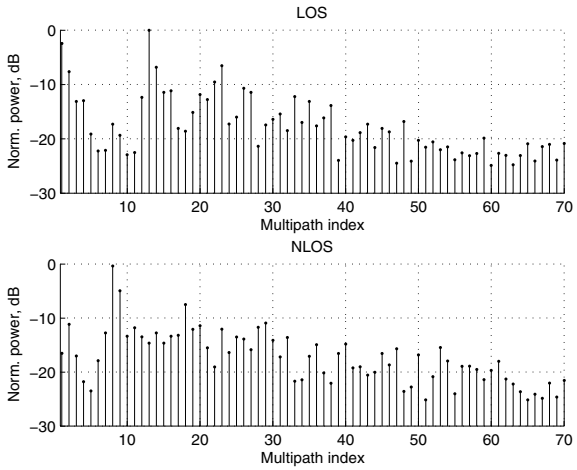

Figure 2. Average multipath profiles for LOS and NLOS channels normalized to the peak mean multipath power

antenna. The cables, connectors and amplifier were calibrated to remove frequency-dependent phase distortion and attenuation. A total of 20,000 channel responses were thus measured.

The complex transfer function obtained at each grid point (x, y) was converted to the channel impulse response through the inverse Fourier transform to obtain

$$\tilde{h}_{x,y,\tau} = \sum_{k=1}^{K} a_{x,y,k} e^{j\varphi_{x,y,k}} \delta_{\tau,\tau_{x,y,k}}, \quad (1)$$

where a and φ represent the magnitude and phase response at the k^{th} time-bin, and τ represents time delay with reference to the first multipath arrival. This was thresholded to 25 dB below the peak power level and squared to obtain the power delay profile (PDP). For each measured PDP, a local peak detection algorithm was used to resolve the multipaths and obtain the multipath profile

$$m_{x,y,l} = \sum_{l=1}^{L} \alpha_{x,y,l} e^{j\varphi_{x,y,l}} \delta_{\tau,\tau_{x,y,l}} \quad (2)$$

where l is the time-bin where a multipath is detected, L is the total number of multipaths in the PDP, and

$$\alpha = a\left(\sum_{k=1}^{K} a_k^2\right)^{-2} \quad (3)$$

is the multipath magnitude with power-normalization to remove pathloss. The average PDP, obtained from a large number of measured or simulated channel impulse responses, is often used to represent the multipath behavior of a channel. An alternative representation used here is the average multipath profile, which is the ensemble mean of the multipath powers in the order of times-of-arrival, i.e.,

$$\bar{m}_l = \frac{1}{n_x n_y} \sum_{x,y=1}^{n_x,n_y} m_{x,y,l}, \quad (4)$$

where l is the multipath index and $n_x = n_y = 100$ is the number of measurement points in each direction for our positioning grid. Fig. 2 shows $\bar{m}_l$ for the LOS and NLOS indoor UWB channels, normalized with respect to the global peak signal level $\max_l\{\bar{m}_l\}$, for L = 70. The first path in LOS is much stronger than that in NLOS because of the presence of the obstruction in the latter. The first cluster in the LOS appears to be missing in the NLOS profile, but the rest of the clusters and rays appear to be largely unaffected from the NLOS blockage and appear in nearly the same order as expected. Multipath clustering can be observed in both scenarios.

Also, from our measurement, the direct path is not always the strongest path in the LOS profile, and indeed the 13$^{\text{th}}$ multipath in Fig. 2(top) has the highest power, which becomes the 8$^{\text{th}}$ path in NLOS, as in Fig. 2(bottom). This observation indicates that the multipath arrivals are not always temporally orthogonal and some degree of multipath overlapping does indeed take place in the indoor channel even with the full UWB bandwidth.

III. SPECTRAL VARIATION

It is well known that the time resolution of a system is inversely related to bandwidth B, which suggests that an increase in B should lead to detection of a higher number of multipaths. This behavior is similar to the greater number of resonant modes observed in a cavity when a wideband excitation is applied. Thus the bandwidth is expected to strongly impact the propagation properties of the channel. The assumption here is that the system is operating in a dense multipath channel with high multipath incidence, so that increasing the temporal resolution continues to result in a proportionate increase in the number of resolved multipaths. This assumption may not necessarily be true for all channels and UWB bandwidths, and will be assessed in this section.

Similarly, frequency-dependent propagation can significantly impact UWB signal propagation. Various propagation modes, such as diffraction and material penetration, are frequency-dependent. It can therefore be expected that the multipath characteristics in different sub-bands within the full channel would be dissimilar.

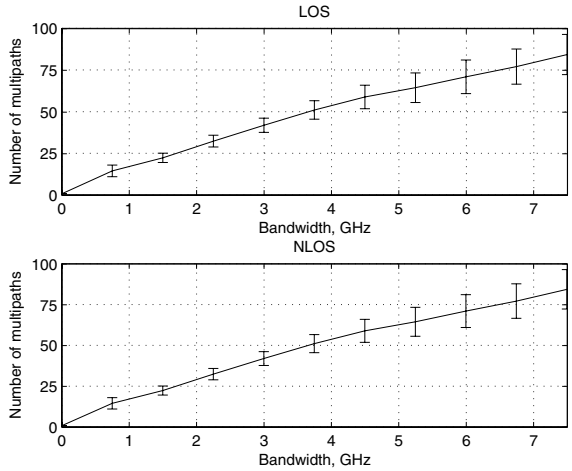

Figure 3. Influence of bandwidth on the number of resolved multipaths. The lines and errorbars indicate the mean and standard deviation

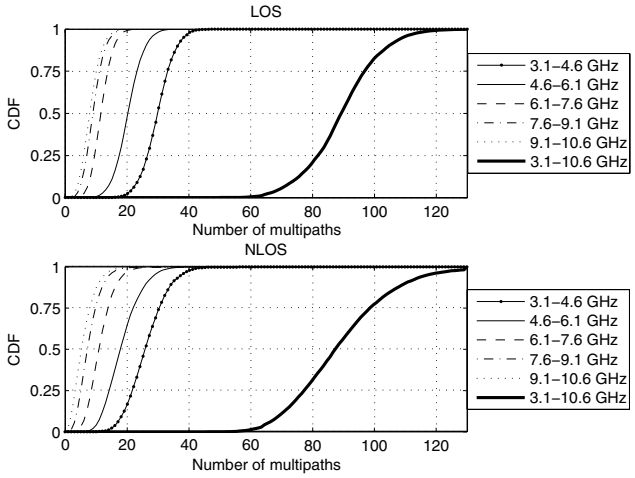

Figure 4. Empirical CDFs of the number of multipaths in the full-band UWB channel and in its five equal sub-bands

A. *Variation with Bandwidth*

From our experimental analysis, the mean number of multipaths L varies approximately linearly with B, as shown in Fig. 3, with slopes of 10.85 and 10.98 paths/GHz for LOS and NLOS channels. The errorbars in the figure indicate that the standard deviation increases with the number of resolved multipaths and bandwidth. This information can be used in choosing the required rake receiver diversity order for single-band or multi-band UWB systems with a given bandwidth. For a full-band UWB system, a mean of about 85 multipaths are observed from our measurements, with a 25 dB threshold.

B. *Sub-Band Comparsion*

Sub-band analysis is performed by dividing the measured 7.5 GHz wide frequency band into $b = 5$ equal sub-bands, each 1.5 GHz wide. The sub-band transfer functions, zero-padded to keep the number of samples constant, are then used to obtain the multipath profiles for the signals contained in those spectral regions. The multipath profiles are thresholded using a 25 dB threshold below the strongest signal level in the full-band impulse response in order to perform a fair comparison. The number of resolved multipaths, L, is used as the test statistic.

The cumulative distribution functions (CDFs) of L_i, $i = 1,\ldots,b$, for each sub-band are shown in Fig. 4. The full-band L CDF is also shown for reference. The full-band L assumes a value that is generally about five times that of L_i, due to the five-fold bandwidth. L_i shows a progressive decrease with increase in the centre frequency. This can be attributed to frequency-selective pathloss induced by omni-directional antennas, which causes the signal in the higher frequencies to undergo greater attenuation and fall below the threshold. The channel frequency selectivity due to the propagation environment also contributes towards the non-uniformity in L_i. Thus the lowest sub-band perceives 20 additional multipaths as compared to the highest sub-band. This observation establishes that the sub-band multipath behavior is non-uniform, and the dependence of multipath propagation on both bandwidth and centre frequency must be taken into account during UWB channel modeling.

IV. Degrees of Freedom

Considering that the multipath arrivals can be represented by discrete random variables with finite probabilities, an effective multipath diversity measure can be obtained in the form of entropy. The entropy H corresponding to the multipath profile at receiver location (x, y) can be calculated as [13]

$$H_{x,y} = -\sum_{l=1}^{L} m_{x,y,l}^2 \log_{L_{x,y}} m_{x,y,l}^2, \qquad (5)$$

and can be used to derive the effective number of multipaths, or the degrees of freedom, i.e.,

$$\hat{L}_{x,y} = L_{x,y}^{H_{x,y}}. \qquad (6)$$

The CDFs of $\hat{L}_{x,y}$ for the measured LOS and NLOS channels are shown in Fig. 5, with mean values of about 27 from our measurement data. This is a high diversity order, and a suitable multipath combining scheme can use it to reduce the outage probability significantly. However, the effective multipath diversity, in terms of the degrees of freedom, is offered by only a fraction of the resolved multipaths, as shown in Fig. 5. The percentage of effective multipaths is calculated as

$$\tilde{L}_{x,y} = \frac{\hat{L}_{x,y}}{L_{x,y}} \times 100. \qquad (7)$$

On average, only about 30% of the resolved multipaths meet this criterion. Depending on the desired performance level of multipath diversity combining, this information can be used to obtain the required complexity for a rake order.

Also, as the multipath degrees of freedom are, on average, much lower than the number of resolved multipaths, it can be inferred that the multipaths have a finite correlation, and the usual assumption of an uncorrelated scattering channel is only applicable to indoor UWB channels as an approximation.

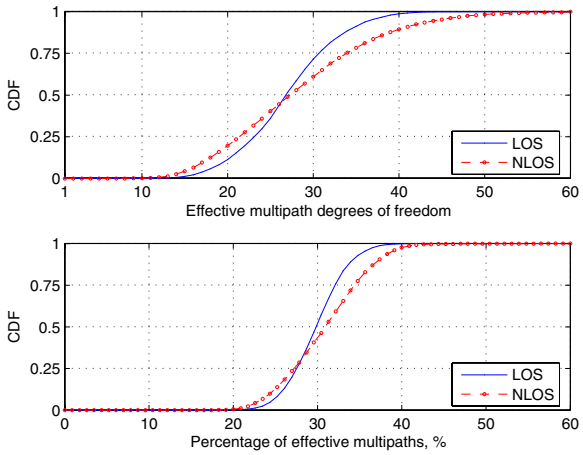

Figure 5. CDFs of the multipath degrees of freedom (top), and the ratio of the degrees of freedom to the number of received multipaths in terms of the percetage derived from each impulse response (bottom)

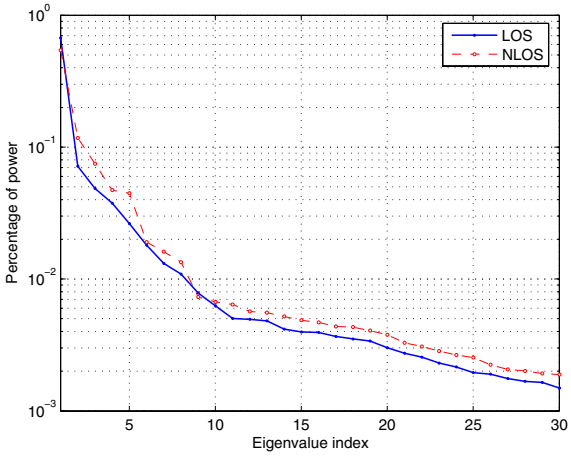

Figure 6. Mean normalised eigenvalues for the first thirty modes and the percentage of the total power that they contained

V. Power Gains

The multipath power gains in a channel determine the relative distribution of power across the multipaths. This provides a measure of the performance of a multipath combining receiver and predicts the upper bounds on its power capture capability. The covariance matrix of the channel with multipath profile $m_{x,y,l}$ is given by

$$\mathbf{K}_{x,y} = E\left[m_{x,y,l} m_{x,y,l}^{\mathrm{H}} \right] \qquad (8)$$

where $(.)^{\mathrm{H}}$ denotes the Hermitian transpose. The empirical covariance matrix for the measured frequency-selective channel is therefore

$$\mathbf{K}_{x,y} = \frac{1}{n_x n_y} \sum_{l=1}^{L} \left(m_{x,y,l} - \bar{m}_{x,y,l} \right) \left(m_{x,y,l} - \bar{m}_{x,y,l} \right)^{\mathrm{H}} \qquad (9)$$

Next, the eigenvalues, λ_i, of $\mathbf{K}_{x,y}$ are computed and normalized such that

$$\sum_i \lambda_i = 1. \qquad (10)$$

The largest non-trivial eigenvalues can be obtained by using a power sum threshold s, such that

$$\sum_{i=1}^{L_s} \lambda_i \le s, \qquad 0 \le s \le 1, \qquad (11)$$

provides an estimate of the number of significant eigenvalues, with the λ_i in descending order. The threshold s is usually taken as 90% or 98%. The 90% L_S for LOS and NLOS are 9 and 13 respectively, while the 98% values are 56 and 62 respectively. The mean eigenvalues for some of the most dominant modes are shown in Fig. 6, illustrating the percentage of power contained in each. Both LOS and NLOS eigenvalues follow an exponential decay with similar decay constants.

VI. Small-Scale Spatial Variation

The evidence of small-scale fading in the UWB channel is provided by spatial variability analysis. This technique also offers an insight into the signal variation resulting from a small relocation of the receiver within the coverage area. Such characterization is immensely useful in the assessment of system robustness. We perform this analysis by inspecting the number of multipaths L at all locations on the measurement grid. The results are displayed in the form of planar intensity plots, such that the transmitter is located to the south of the synthetic aperture array in its far field, as illustrated by Fig. 1.

Fig. 7 shows alternating regions of high and low L in a planar region, forming a standing wave pattern. The horizontal high-L lines are aligned with the wavefronts of the direct path, as can be inferred from a comparison with Fig. 1. The lines are present in both LOS and NLOS. In the latter, a strong diagonal pattern is also superimposed, which arises from a corner reflection. This suggests that the pattern is dependent on the room geometry, the location of the transmitter, and the presence of the direct path. This pattern is formed due to the Lloyd's mirror phenomenon [14]. The higher contrast in NLOS indicates the greater variation of the number of multipaths at various locations. The sharp variation in L implies that the total received power is not constant over an area, and fading is present. The standing wave pattern has a 4 cm wavelength, which corresponds well to the signal bandwidth B = 7.5 GHz.

This pattern can be used to determine the optimal antenna separation for a two-branch diversity system. In such a system, it would be desirable to place the antennas at such a distance that at least one of them is in a low fade position at any given time but with sufficient separation to obtain uncorrelated small-scale fading across the branches. From the interference patterns for a full-band UWB system, this optimal spacing is equivalent to half a wavelength of the fading standing wave, i.e. about 2 cm. Thus this simple analysis shows the feasibility of compactly placed diversity antennas in UWB systems. If a multi-band UWB signal with a relatively smaller bandwidth is

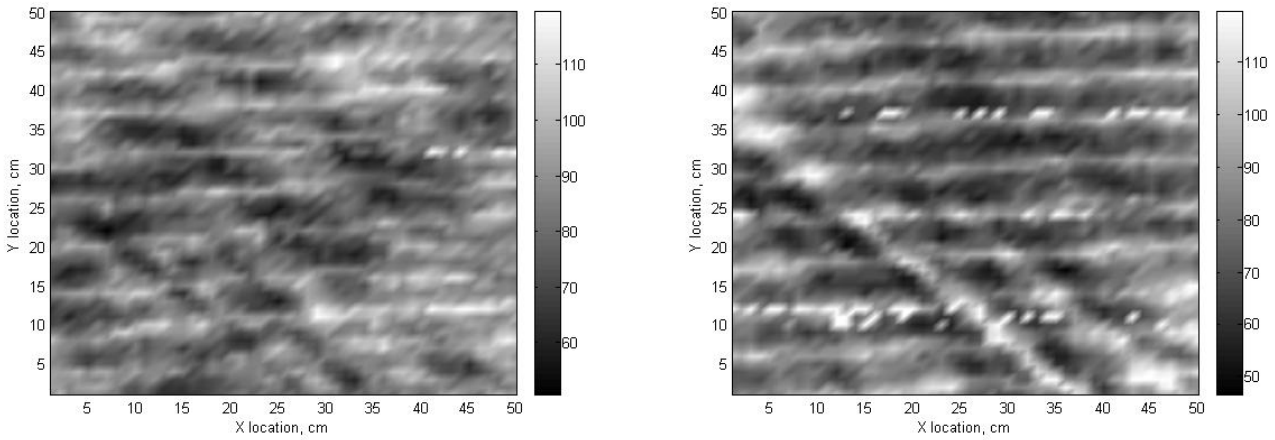

(a) (b)

Figure 7. Spatial variation of number of received multipaths in a 0.5 m x 0.5 m area for (a) LOS and (b) NLOS scenarios. The transmitter is located to the south of the synthetic aperture in the far field. A standing wave pattern with wavelength corresponding to the signal bandwidth is obtained

used, however, this distance will be proportionately larger. Also, the power captured by a rake receiver increases with the number of resolved multipaths incident at the receiver, assuming a high diversity order. Thus the performance of a rake would also vary with a small movement of the receiving antenna, according to Fig. 7. From the relationship between the bandwidth and the wavelength of these standing waves, it can be inferred that relatively narrowband systems would have larger regions with such variations, as suggested in [15]. Conversely, with an even wider signal, these interference fringes would be closer together, so that in the infinite bandwidth limit there would be a spatially uniform distribution of L and no small-scale fading, as is observed with optical signals for instance.

VII. CONCLUSION

Multipath propagation in indoor ultra-wideband channels has been characterized experimentally and the implications for efficient system design have been considered. The number of resolved multipaths, L, is shown to increase linearly with bandwidth with a slope of 11 paths/GHz. In different sub-bands within the UWB frequency range, L falls monotonically with increase in the centre frequency. From our measurement, the received multipaths have approximately 27 degrees of freedom – about 30% of the number of resolved multipaths – which provides an estimate for the required rake fingers to achieve near-optimal SNR gain in a given multipath channel. The optimal antenna separation for diversity systems is found to be 2 cm for a full-band UWB system, increasing at lower bandwidths. Thus UWB systems can use compact diversity arrays to combat small-scale fading. This work provides a framework for the design of channel-optimized UWB systems.

REFERENCES

[1] M. Z. Win and R. A. Scholtz, "Charaterization of ultra-wideband wireless indoor channels: a communication-theoretic view," *IEEE J. Select. Areas Commun.*, vol. 20, Dec. 2002.

[2] S. S. Ghassemzadeh, R. Jana, C. W. Rice, W. Turin, and V. Tarokh, "Measurement and modeling of an ultra-wide bandwidth indoor channel," *IEEE Trans. Commun.*, vol. 52, Oct. 2004.

[3] W. Q. Malik, C. J. Stevens, and D. J. Edwards, "Synthetic aperture analysis of multipath propagation in the ultra-wideband communications channel," in *Proc. IEEE SPAWC*. New York, USA, June 2005.

[4] A. F. Molisch, "Ultrawideband propagation channels - theory, measurement, and modeling," *IEEE Trans. Veh. Technol.*, 2005 (in press).

[5] W. Q. Malik, D. J. Edwards, and C. J. Stevens, "Angular-spectral antenna effects in ultra-wideband communications links," *IEE Proc.-Commun.*, (in press).

[6] W. Q. Malik, D. J. Edwards, and C. J. Stevens, "The impact of physical layer frontend characteristics on ultra-wideband radio," in *Proc. 12th Int. Conf. Telecom.* Cape Town, South Africa, May 2005.

[7] T. S. Rappaport, *Wireless Communications: Principles and Practice*, 2nd ed: Prentice Hall, Dec. 2001.

[8] R. J.-M. Cramer, R. A. Scholtz, and M. Z. Win, "Evaluation of an ultra-wide-band propagation channel," *IEEE Trans. Antennas Propagat.*, vol. 50, May 2002.

[9] W. Q. Malik, M. C. Mtumbuka, D. J. Edwards, and C. J. Stevens, "Performance analysis of ultra-wideband spatial MIMO communications systems," in *Proc. IST Mobile Comm. Summit*. Dresden, Germany, June 2005.

[10] M. C. Mtumbuka, W. Q. Malik, C. J. Stevens, and D. J. Edwards, "Performance of spatial diversity in ultra-wideband systems," *IEE Proc.-Commun.*, (in press).

[11] W. Q. Malik, M. C. Mtumbuka, C. J. Stevens, and D. J. Edwards, "Increasing MIMO capacity in ultra-wideband communications through orthogonal polarizations," in *Proc. IEEE SPAWC*. New York, USA, June 2005.

[12] W. Q. Malik, D. J. Edwards, and C. J. Stevens, "Experimental evaluation of Rake receiver performance in a line-of-sight ultra-wideband channel," in *Proc. Joint IEEE UWBST & IWUWBS*. Kyoto, Japan, May 2004.

[13] F. Patenaude, J. Lodge, and J.-Y. Chouinard, "Eigen analysis of wide-band fading channel impulse response," *IEEE Trans. Veh. Technol.*, vol. 48, Mar. 1999.

[14] E. Hecht and A. Zajac, *Optics*, 4th ed. London, UK: Addison-Wesley, 2001.

[15] M. S. Varela, M. G. Sanchez, L. Lukama, and D. J. Edwards, "Spatial diversity analysis for digital TV systems," *IEEE Trans. Broadcast.*, vol. 47, Sept 2001.